Energimyndighetens titel på projektet – svenska Distribuerade fjärranslutna mätare för aktiv estimering av nätparametrar i realtid för digitala elkraftssystem
Energimyndighetens titel på projektet – engelska Distributed remote meters for active estimation of real-time grid parameters for digital electric power systems
Universitet/högskola/företag: Chalmers Tekniska Högskola — Avdelning/institution: Elektroteknik/ Elteknik
Adress Hörsalsvägen 11, 412 96 Göteborg
Namn på projektledare Massimo Bongiorno
Namn på ev övriga projektdeltagare Azam Bagheri (author of this report)
Nyckelord: 5-7 st Frequency-Dependent Grid Impedance, Machine Learning, Long-Short-Term Memory (LSTM), Random Forest (RF)

Förord

This PostDoc project has been sponsored by Energimyndigheten together with ABB Corporate Research Center (today Hitachi Energy) and Chalmers Area of Advance. The project has been extensively discussed with industrial partners. Prof. Jan R. Svensson, ABB Corporate Research/Hitachi Energy research and Adjunct Professor at Chalmers, has been extensively involved in supervision of the PostDoc.

Innehållsförteckning

Box 310 • 631 04 Eskilstuna • Besöksadress Kungsgatan 43
Telefon 016-544 20 00 • Telefax 016-544 20 99
registrator@energimyndigheten.se
www.energimyndigheten.se
Org.nr 202100-5000

Sammanfattning

Syftet med projektet är att utforska vilka möjligheter ett överlagrat kommunikationssystem tillför framtidens kraftelektroniksdominerande elkraftssystem. Mer specifikt kommer projektet att fokusera på lokala/distribuerade fjärrmätningar för att uppskatta viktiga systemparametrar för att få en ökad observerbarhet i elkraftssystemet. Mätningarna kommer att användas för att uppskatta den frekvensberoende impedansen hos elkraftssystemet sett från en specifik anslutningspunkt. Olika systemförhållanden, från stationära till dynamiska tillstånd orsakade av större störningar, till exempel kortslutningar, kommer att utvärderas. Olika metoder för att uppskatta den frekvensberoende impedansen kommer att analyseras och jämföras. Projektets slutmål är att tillhandahålla förståelse och ett system av algoritmer för att i realtid uppskatta kraftsystemets impedans vid en specifik anslutningspunkt för ett stort frekvensområde, vilket kan användas för en mer robust styrning av nätanslutna omriktare.

Summary

The aim of this project is to exploit the opportunities that an extensive layer of communications will bring in the future power-electronic dominated power system. In particular, the project focus is on using local and remote measurements for system parameter estimation to enhance the observability of the power system. The acquired measurement information will be used to estimate the frequency-dependent impedance of the power system seen from a specific connection point. Several system conditions, from steady-state to fast dynamics due to large disturbances, i.e., short-circuit faults, will be considered and investigated. Different estimation methods will be analyzed and evaluated. The final goal of the project is to provide a fast-online measurement of the power system impedance at a specific connection point for a wide-frequency range, to be later used for robust control of grid-connected converters.

Inledning/Bakgrund

The high penetration of renewable energy sources into the power grids is leading to a widespread use of grid-connected power converters throughout the entire system. As a result, the reliability and stability of the overall power system is more and more dependent on the specific control strategy and parameters of the different converter units. The equivalent grid impedance at the converter's connection point (or grid strength) can influence the parameters of the converter control system for optimal performance on speed, robustness and reliability [1][2][3].

Today many new technologies are available, especially in the information and communication technology (ICT) sector, which might allow to enable more efficient and effective solutions than the traditional ones. In the future, there will be a need for advanced technologies, especially involving the integration of ICT and

the power electronics for planning, managing, monitoring, controlling and delivering electricity in a safe and reliable way. Meanwhile, increasing the flexibility and efficiency of the power system. This is the core of the digitalization process of the electric power systems, where the combination of advanced power technology together with an extended layer of communication will enable to increase the performance of the power system by taking advantage of the observability introduced by the ICT and the controllability offered by the different power-electronics based devices connected to the system.
Modern measurement systems and, particularly, communication systems (i.e., based on 5G technology) open up new possibilities to provide the controllers with more information on the surrounding environment. Today, the power system is already provided by several dedicated measurement equipment, such as energy meters and Phase Measurement Units (PMUs). In the future, it is possible to imagine that system measurements will not only be provided by dedicated units. Any grid-connected converter (HVDC, FACTS, wind turbine converters, solar PV inverters, etc.) that is already equipped with high-bandwidth current and voltage sensors for local control. Thanks to ICT, it is possible to assume that these sensors will be used as remote measurement points and relevant information can be shared among different power-electronic devices for monitoring and control purposes, as depicted in Figure 1. Thus, this new kind of "ancillary service" will reduce the need for installing new measurement units. However, the converters need to be equipped with a standardized communication unit that handles time-stamped data (for example, through a GPS signal) to synchronize the spread-out measurement locations. When more relevant measured signals are provided to the control process, the need to use feedback signals to handle system uncertainties (model errors, non-modelled subsystems, external disturbances etc.) in the process decreases. This would not only enhance the controllability of the power converters, but would also make the system more robust against system disturbances and at the same time reduce the risk for induced stability problems and control/hardware interactions [4].

In a longer perspective, the wide-spread use of power-electronic converters will add new requirements on the implemented control systems. It is not sufficient that the regulated quantity tracks its reference value despite of disturbances that appear in the system or in the short-circuit power level of the system. The control system must be designed so that it does not interact in an adverse way with other converters connected to the same power system. Thus, it should be possible to install new devices without the need of re-tuning the controllers of the existing ones.

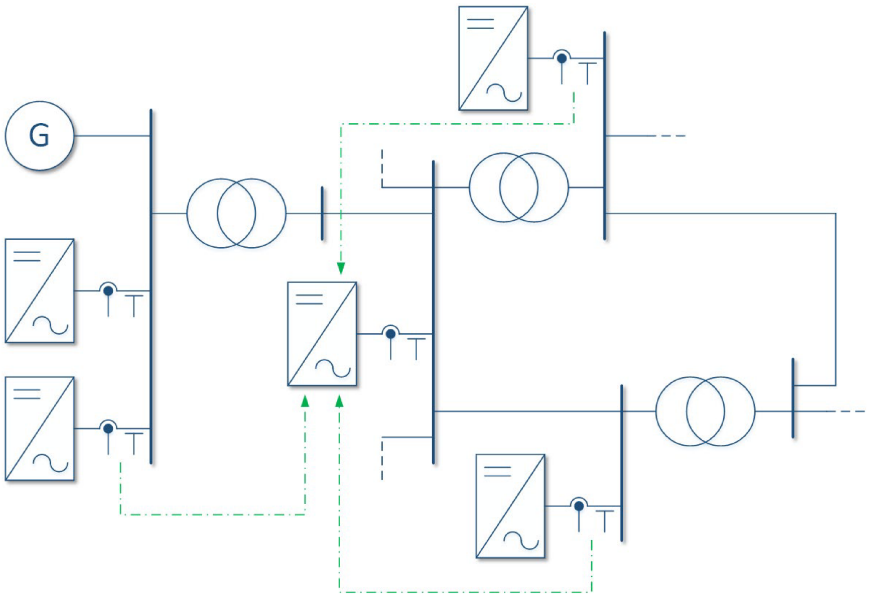

Figure 1. Example of power-electronics dominated grid with communication (green lines) between converters

It is under this scenario that this project aims at developing Artificial Intelligence (AI) based methods to analyze the use of local and remote measured data to estimate the frequency-dependent grid impedance at a specific location of the grid. At an early stage of the project, an extensive literature review has been performed on the existing grid impedance estimation methods. This study has shown that the existing methods fall short in dealing with a large amount of data, especially time-series data. Further, impedance estimation methods that use the Discrete Fourier Transform (DFT) to extract harmonic impedance must comply with DFT limits (e.g., Nyquist frequency, need for use of windowing techniques, etc.), and they have limited functionality during transient conditions, especially when dealing with very high-speed transients such as short-circuit faults. This project proposes the use of an AI-based approach to address the above-mentioned issues. The applied method is a mixture of deep learning (DL) and machine learning (ML) techniques. Since the input signal is a three-phase time-series data (three-phase voltages/currents), a long-short-term-memory (LSTM) technique is applied for feature extraction purpose, and a random forest (RF) method has been used to map the extracted features by LSTM model to the grid impedance, which is calculated analytically. The results show the effectiveness of the proposed method for estimating the frequency-dependent grid impedance for a wide range of frequencies.

According to the obtained results, remote measurement of three-phase voltage /current signals is essential to estimate grid impedance more accurately. Thereby, the next step is to find out the optimum location and numbers of remote measurement nodes to increase the accuracy of the proposed method.

Several grid impedance estimation methods have been proposed in the literature, which can be divided into passive and active methods [3][5]. The passive methods operate at steady-state condition as state-estimators of the fundamental frequency.

Most often they use time-domain voltage and current data as inputs and algorithms such as least-squares [6], Kalman filters (i.e., the Kalman filter models only fundamental frequency) [7], wavelets [8] to estimate the Thevenin model of the power grid. On the other hand, active methods aim at detecting the grid impedance for range of frequencies. Active methods mainly consist of two types: invasive [9][10] and non-invasive ones [11]. The non-invasive methods use some existing harmonic sources due to large disturbances (e.g., electrical faults, nonlinear load switching, transformer/ capacitor energizing, power converter switching, and many more) to indicate the frequency-dependent power grid impedance around the oscillation frequencies. Kalman filters (i.e., the Kalman filter models several harmonic frequencies) [12], machine learning-based regression methods [13] are examples of practical non-invasive ones.

Invasive methods use the direct injection of the broadband excitation signal, followed by data acquisition and finally applying signal processing techniques to estimate the corresponding impedance at all exciting frequencies. The popular broadband excitation signal in steady state is pseudo random binary sequence (PRBS) signal [5][14].

The magnitude of the excitation signal needs to be appropriately designed to extract the impedance variations. The desired magnitude of PRBS should be small enough to ensure that the system stays around its operating point. However, it should be sufficiently large to reject noise disturbances. In general, the magnitude of the excitation signal is chosen between 5% and 10% of steady-state values [5].

The main challenge of active methods is time burden since the active method uses discrete Fourier transform (DFT) to extract the frequency components of the measured data. DFT needs at least one cycle of data for each frequency component, resulting in considerable computation burden especially for estimation in the lower cycle frequencies. Moreover, to cope with noise impact, the signal injection should be repeated several times or applied for more cycles [5]. Further, during transient state, the signal injection approach is not effective since the background harmonics (i.e., nonstationary harmonics and phase-shifted harmonics) change during the estimation process [15].

The aim of this project is using deep learning techniques to estimate the grid impedance at both steady-state and transient conditions of the power grid. In particular, the goal is to propose an unsupervised sequential deep learning method, LSTM-Autoencoder (LSTM-AE) with a dedicated architecture, to extract time-dependent feature vector sequences from measured data at several locations of the power grid. A random forest (RF) regressor is then employed to estimate the frequency-dependent grid impedance during large disturbances. It is shown that using the extracted feature sequences instead of original data sequences leads to improved grid impedance estimation. To test the effectiveness of the proposed scheme, a grid-connected power converter is simulated, where voltage and current time-series are collected at local and some other remote points. The collected data sequences are then fed into the proposed scheme for feature extraction and frequency-dependent impedance estimation.

Genomförande

The project has been conducted based on a pre-defined time plan that has been closely followed. Generally, detailed studies have been done on various methods for grid impedance estimation and they are implemented in MATLAB simulation environment to compare their results with proposed method. The same simulation setup was applied to generate synthetic local and remote data and conducting comparative analysis. The proposed method implemented in TensorFlow/Keras environment. The results are provided by Azam Bagheri (Postdoc at Chalmers), in cooperation with Prof. Massimo Bongiorno (project leader, Chalmers) and Prof. Jan R. Svensson, Hitachi Energy Research (earlier ABB Corporate Research) and Adjunct Professor at Chalmers. Together with this report, outcome from this project are one journal and two conference publications.

Proposed Method

To estimate the grid impedance, the basic idea is to use unsupervised automatic feature learning technique to extract the sequences of time-dependent features of dynamic power grid data. Given time-dependent features, a nonlinear regression method is exploited to derive a nonlinear function that maps the features to the corresponding grid impedance phasor.

Simulation Setup

Based on mentioned idea we propose a new scheme as shown in block diagram of Figure 2. The red dash box in Figure 2 shows a utility power grid system used to generate synthetic data for training introduced modules. The blue dash box shows two main modules of the proposed method as follows:

1. An LSTM-AE architecture [16] for unsupervised automatic learning of time-dependent feature sequences form dynamic power grid data (e.g., symmetrical components of three-phase voltage and current data);
2. A non-linear RF regression method for estimation frequency-dependent grid impedance. The RF regressor takes the features extracted by LSTM-AE module as an input and derives a nonlinear map function between input feature and values of grid impedance in wide range of frequency.

The inputs to the blue box are time-series three-phase voltage/current data and the output is grid impedance seen from bus B1 for a wide range of frequencies, namely $Z(\mathrm{j}\omega)$. Further, details of the individual modules are given in the following part of this report.

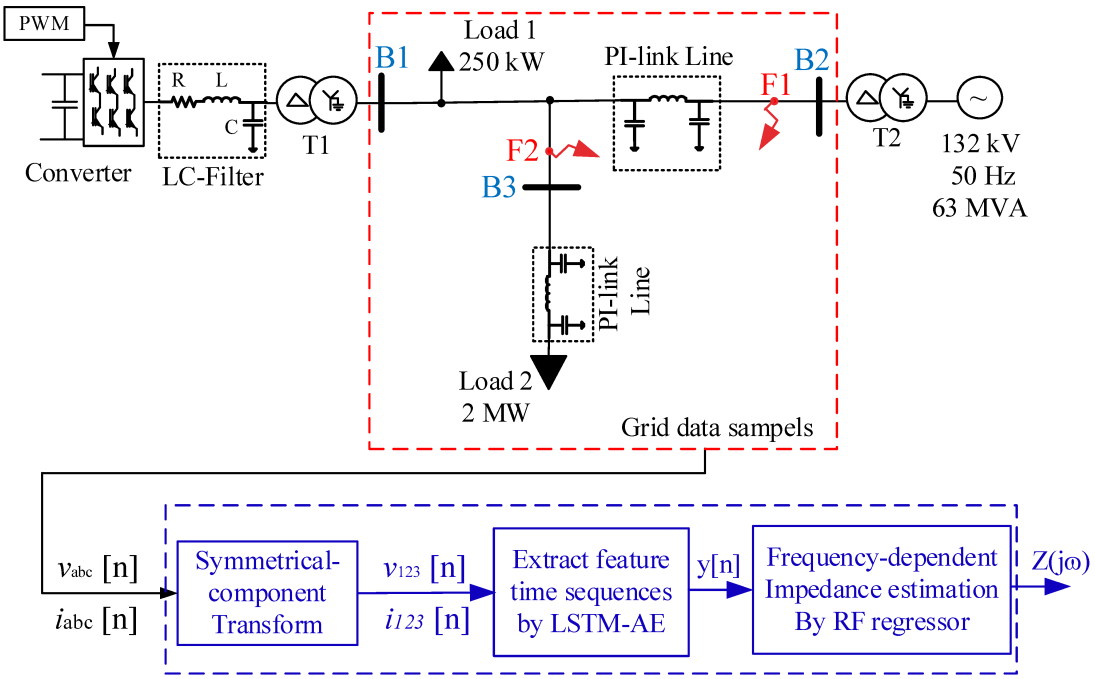

Figure 2. The overall schematic of the proposed method: power grid (red dash line box), the deep learning-based nonlinear estimator (blue dash line box).

Measurement Data

To estimate the grid impedance seen from node B1 in Figure 2, the three-phase voltage and current data are measured at that node and two other remote nodes (B2 and B3 in Figure 2) of the power grid. The discrete sampled three-phase signals are transferred into symmetrical components through:

$$\begin{bmatrix} \boldsymbol{x}_1[n] \\ \boldsymbol{x}_2[n] \\ \boldsymbol{x}_0[n] \end{bmatrix} = \frac{1}{3}\begin{bmatrix} 1 & a & a^2 \\ 1 & a^2 & a \\ 1 & 1 & 1 \end{bmatrix}\begin{bmatrix} \boldsymbol{x}_a[n] \\ \boldsymbol{x}_b[n] \\ \boldsymbol{x}_c[n] \end{bmatrix} \quad (1)$$

where n is the sampling point in the time domain, $\boldsymbol{x}_{\mathrm{a}}[n]$, $\boldsymbol{x}_{\mathrm{b}}[n]$ and $\boldsymbol{x}_{\mathrm{c}}[n]$ are the discrete three-phase time-series voltage and current phasors, $\boldsymbol{x}_1[n], \boldsymbol{x}_2[n]$, and $\boldsymbol{x}_0[n]$ are the corresponding discrete positive-, negative- and zero-sequence components, respectively, and $a = \mathrm{e}^{(\mathrm{j}2\pi/3)}$.

The measurement duration is one grid cycle (20 ms at 50 Hz), and the sampling frequency is 10 kHz. At each point, we measure both voltage and the current phasors, resulting in 18 different features. To synthesize the training dataset we increased the r, l, and c parameters of the PI-link model of the transmission lines gradually by 10% through 3 nested loops. For each new value of parameters, we collect the measurement data at local and remote nodes as input features. In addition, we measured magnitudes and angles of the corresponding grid impedance at node B1 using the sin-sweep method [17]. The sweep frequency range starts from 5 Hz through 765 Hz using frequency interval of Δf =5 Hz.

Feature extraction from data sequences by LSTM-AE

To automatically learn the time-dependent sequential features from the measurement data, a LSTM-AE module is exploited. Dealing with time-series, recurrent neural networks (RNN) and especially the LSTM networks are shown to be the suitable choices [18]; furthermore, LSTM-AE is particularly suitable for unsupervised learning of data sequences [19].

In the proposed LSTM-AE architecture the encoder consists of one input layer and two LSTM-AE layers (see Figure 3(a)). The LSTM-AE layers contain 16 and 8 units, respectively. Each LSTM layer followed by a nonlinear activation function ReLU (Rectified Linear Unit).

The original 2D matrix $\boldsymbol{X}$ (i.e., 200 samples of 18 features), obtained from (1), is reformed into 3D by partitioning one cycle data into 10 sub-cycles (i.e., $\{\boldsymbol{X}\}_{200\times18} = \{\{\boldsymbol{X}_0\}_{20\times18}, \ldots . \{\boldsymbol{X}_9\}_{20\times18}\}$). As shown in Figure 3(a), the input layer takes 1st sub-sequence $\boldsymbol{X}_0 = \{\boldsymbol{s}_0, \ldots, \boldsymbol{s}_{19}\}$ and applies it to the 1st layer. The output of 2nd layer extracts the sequential features of current sub cycle denoted by $\boldsymbol{y}[n]$.

Figure 3(b) shows that applying each sub-sequence of one cycle data to the encoder results in one sequence of time-dependent features. We concatenated these 10 feature-sequences and provided them to RF regression module as the input.

Table 1 summarizes the architecture of the proposed LSTM-AE and Figure 3(c) shows the block diagram of proposed LSTM-AE model. Since the decoder part is only applied during the training where its structure is the exact inverse form of the encoder, the information of the decoder is not included in the table. In the LSTM-AE, learning encoder coefficients are obtained through feedforward neural network manner. Let the feature vector obtained from the encoder be:

$$\boldsymbol{y}[n] = f(\boldsymbol{b} + \boldsymbol{W}\boldsymbol{x}[n]) \tag{2}$$

where $\boldsymbol{x}[n]$ is the time-dependent input data, $f(\cdot)$ is a nonlinear function, $h(\boldsymbol{x}[n]) = \boldsymbol{b} + \boldsymbol{W}\boldsymbol{x}[n]$ is the impulse response of a linear system. The decoder is the revers of the encoder ($f^{-1}(\cdot)$) which aids in minimizing the overall error or the loss function, given in (3) during the training, [20],

$$\mathrm{e} = \frac{1}{N}\sum_{n=1}^{N} \|\boldsymbol{x}[n] - \hat{\boldsymbol{x}}[n]\|_2^2 \tag{3}$$

where $\boldsymbol{x}[n]$ is an input data to the encoder, and $\hat{\boldsymbol{x}}[n]$is the reconstructed data from the decoder.

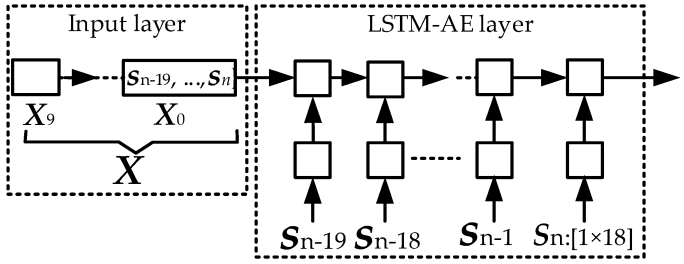

(a)

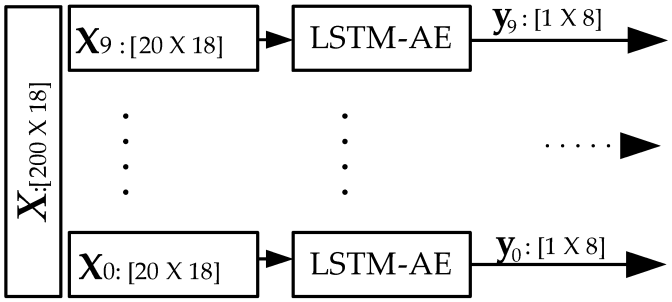

(b)

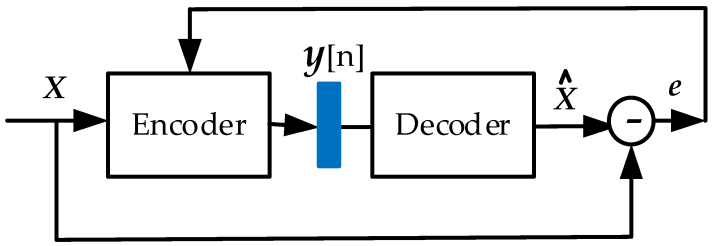

(c)

Figure 3. The proposed LSTM-Autoencoder; a) the overall architecture of LSTM-AE (input layer + 1 LSTM-AE layer); b) concatenating 10 sequences of time-dependent features extracted for 1 cycle data c) the LSTM-AE architecture during training process

Table. 1. Architecture of the Encoder of the Proposed LSTM-AE.

Layers	# Cells	# units / cell	Unit Input	Unit Output
Input layer [20 × 18]		-		-
LSTM-AE 1+ReLU	20	16	20×18	20×16
LSTM-AE 2+ReLU	20	8	20×16	1 × 8

Frequency-dependent grid impedance estimation using RF Regressor

We exploited a RF regression method to derive a nonlinear function that maps the input features to the frequency-dependent grid impedance.

A decision tree regression model has the lowest time complexity in compare with RF and support vector machine (SVM) regression models, but it suffers from high variances [21]. The SVM regression is slower than the random forest, in addition, it does not show sufficiently high performance when dealing with multi-dimension data [21].

A RF consists of a set of decision trees for ensemble average, to obtain the best classification/estimation results [22]. Although the ensembling slows down the RF but it reduces the high variance of individual trees and leads to precise prediction of power system data. Given a set of input feature vectors, a RF subdivides randomly the feature vectors into several subsets where each subset includes all feature columns of original data, and then assigns each subset to one decision tree [22][23]. The decision trees grow by splitting on feature column that maximizes the objective function (e.g., information gain) at that split. The splitting at each node is repeated until the number of samples in the node becomes smaller than a pre-defined value. The final selected nodes (leaves) in the trees are the outputs of decision trees. The estimate from a RF can then be obtained by averaging over the predictions of individual decision trees [24].

Figure 4 shows the overall schematic of the RF regressor block. The proposed RF regressor consists of 50 decision trees where the depth of each tree can grow till maximum 25 states. In our RF regressor, the input is the features of voltage and currents extracted by the LSTM-AE. Then, each decision tree estimates the magnitudes and angles of the grid impedance at desired frequency range. Finally, the grid impedance ($\boldsymbol{z}(\mathrm{j}\omega)$) determined by taking the average of these individual estimations ($\boldsymbol{z}_i(\mathrm{j}\omega)$) where, $\omega = 2\pi f$ denotes the angular frequency where f is ranging from 5 Hz to 765 Hz with frequency interval Δf =5 Hz.

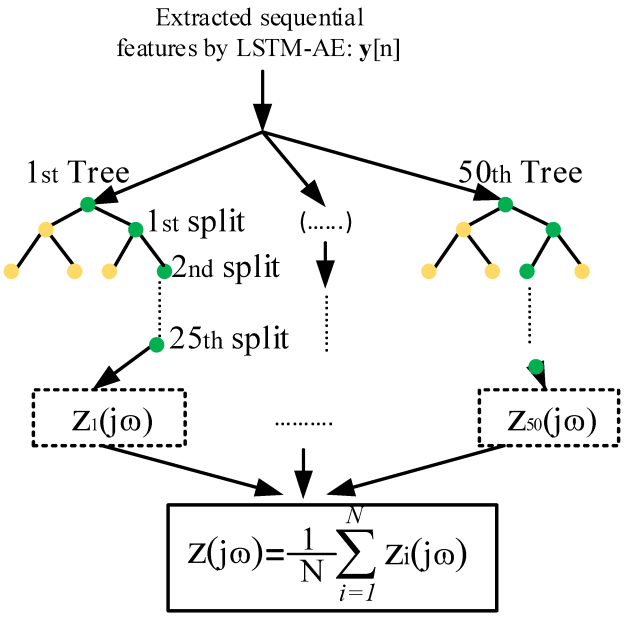

Figure 4. Decision trees of RF regressor, obtained from the training process of the proposed scheme.

Simulation results

In this project we used MATLAB/ Simulink environment for generating synthetic data, as shown in Figure 2 (red dash box). The model consists of a 33kV utility grid connected to the 132kV transmission grid though the step-up transformer T2. In addition, a three-phase AC/ DC converter is connected at the 33 kV bus B1 through a second-order *LC* filter and the step-up transformer T1. The simulated utility grid supplies two three-phase loads rated 250 kW (Load 1) and 2 MW (Load 2). Table 2 lists the parameters of the simulated power grid.

Table. 2. The detailed parameters of the simulated power network.

Description	Values
Overhead line (positive seq.), $l_1, c_1, r_1,$	1.05 mH, 0.33 μF, 0.1153 Ω
Overhead line (zero seq.), $l_0, c_0, r_0,$	3.32 mH, 5.01 nF 0.413 Ω
Load 1: voltage, P	33 kV, 250 kW
Load 2: voltage, P	33 kV, 2 MW
Converter: DC link voltage, f_{pwm}, S	600 V,1980 Hz, 250 kVA
Transformer 1: V_1/V_2, S	415 V/33 kV, 250 kVA
Transformer 2: V_1/V_2, S	132/33 kV, 63 MVA

Datasets

Two synthetic datasets were generated. The first dataset (training dataset) was generated from the power grid under the steady-state condition. The second dataset (test dataset) was correspondent to transient situations like load change or electrical faults (i.e., 400 different three-phase faults occurred at either fault locations F1 or F2). To generate large synthetic dataset, the transients (either load changes or electrical faults) were repeated where the transmission line parameters were changed slightly.
For both datasets, the measurement nodes were at buses B1, B2 and, B3, respectively, shown in Figure 2. At each measurement node. We used the first dataset for training, and the second dataset for testing.

- Training Dataset (Dataset 1): The training dataset, i.e., the first dataset (generated from the power grid in steady state), consisted of 2000 measurement sets. Each set contained 1 cycle (200 samples) of 18 different voltage and current streams (i.e., 3 locations, each location contained 3 voltages and 3 currents). The first dataset was then split according to 60% (1200 measurement sets) and 40% (800 measurement sets) for the training and the validation when training the LSTM-AE model.
- Test dataset (Dataset 2): The overall test dataset include 600 measurement sets which is divided into 3 different subsets. First subset includes 200 measurement sets were collected when power grid is in steady-state and Load 1 (250 kW) was changed gradually for 20% pu. The second 200 measurement sets were collected when fault occurred at fault location F1,

and the rest 200 measurement sets were collected when the tree-phase electrical faults occurred at fault location F2 (see. Figure 2).

It is important to note during collecting each datapoint, as mentioned, the transmission line parameters were changed slightly thereby, the fault impedance and the grid impedance were changed consequently. The details of training/ validation/testing for LSTM-AE and RF regression models are shown in Table 3.

Table. 3. The Size of Training /Test Datasets for both LSTM-AE and RF Regression Models.

Dataset	Size	Models	
		LSTM-AE	RF
Training (Dataset 1)	Input size	[1200, [10, 20], 18]	[1200, 80]
	Output size	[1200, [10, 20], 18]	[1200, 306]
Validation (Dataset 1)	Input size	[800, [10, 20], 18]	[800, 80]
	Output size	[800, [10, 20], 18]	[800, 306]
Testing (Dataset 2)	Input size	[600, [10, 20],18]	[600, 80]
	Output size	[600, [10, 20],18]	[600, 306]

Hyperparameters

The output of LSTM-AE were the 2000 feature vectors (i.e., corresponding to 2000 data points) where each vector contained 80 components. The output of trained RF regressor was the estimated grid impedance matrix, with 2000 rows (corresponding to 2000 data points) and 306 columns including magnitudes and angles of frequency-dependent grid impedance ($\boldsymbol{z}(\mathrm{j}\omega)$). There were several hyperparameters in LSTM-AE and RF regressor. Hyperparameters of the LSTM-AE were optimizing learning rate (lr), the number of LSTM layers, and the number of units in each LSTM layer. After several experiments we decided to use 2 LSTM layers to construct the encoder part where layers have 16 and 8 units, respectively.

Table. 4. Finding the best RF structure that minimizes MSE values through Grid Search

	Depth of trees		
# Decision trees	10	25	50
25	20.0	8.32	7.13
50	5.46	**3.20**	4.86
75	9.14	8.41	9.69
100	5.37	6.36	8.80

In the experiments, the learning rate was lr =0.001, number of $epochs$ =200, and the $batch\ size$= 50. For RF regression, grid search was conducted to find the best

number of random states and the number of estimators according to the MSE criterion. Table 4 shows the results from the grid search, where the smallest MSE was achieved when the number of decision trees was 50, and the depth of decision tree is 25.

Results and performance evaluation

Training and validation of LSTM-AE network

The proposed LSTM-AE architecture was trained and validated from the training dataset, and subsequently used for extract feature vector sequences from the test dataset. To show the proposed LSTM-AE performance, Figure 5 shows the training and validation accuracy as well as the loss, obtained by (3), as a function of epochs. Observing the training curves, one can see that training/validation has reached about 95% accuracy without showing significant difference, indicating there was no obvious overfitting.

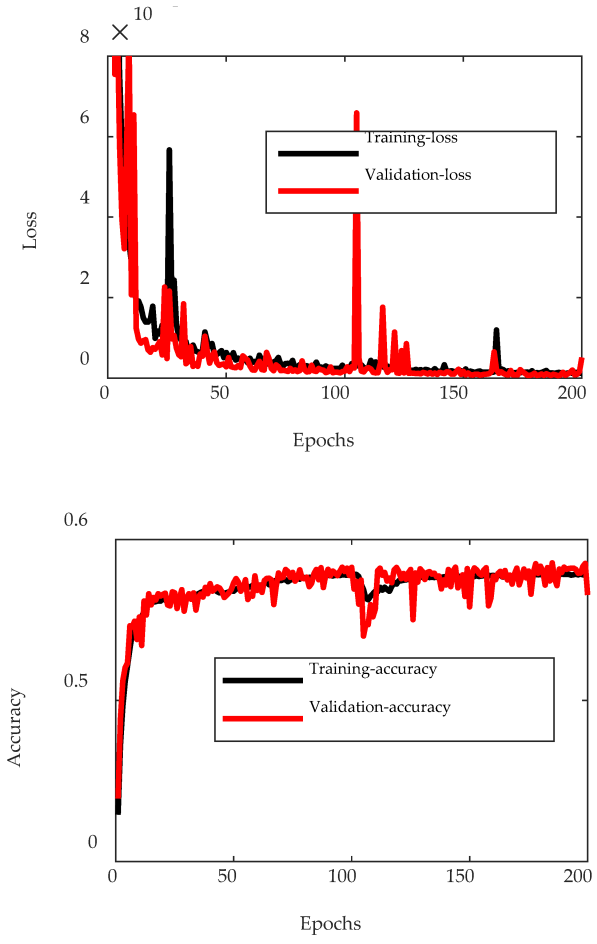

Figure 5. Performance from the training and validation in the proposed LSTM-AE. (top) loss versus epochs, (bottom) accuracy versus epochs.

LSTM-AE network Performance on Grid Impedance Estimation

To verify the proposed estimation scheme, five case studies were conducted. The aim of these studies was to evaluate different aspects of performance, in both steady-state and transient conditions. The case studies verify several aspects of performance of the proposed method including:

1. the performance of the proposed method for estimating variations of the grid impedance magnitude at fundamental frequency (50 Hz) due to load variations;
2. the performance of entire proposed scheme when input data sequences included both local and remote measurements;
3. the effect of using extracted features instead of using original data sequences;
4. the impact of adding measured data sequence from additional remote nodes on the performance of the proposed scheme;
5. performance comparison of the proposed scheme with PRBS signal injection method [5] in terms of accuracy, frequency resolution, and speed.

In all case studies, the performance evaluation criterion for the proposed scheme was the mean square error (MSE) measure as:

$$MSE_i = \frac{1}{N}\sum_{i=1}^{N}(z_i - \hat{z}_i)^2 \quad (4)$$

where z_i and $\hat{z}_i$ are the ith ground-truth and predicted grid impedance values, respectively and N is total number of values.

Case Study 1: Estimation of grid impedance at fundamental frequency

The first case study aimed at verifying the performance of proposed method for estimating the grid impedance magnitude, at fundamental frequency, due to load changing in steady-state condition. The three-phase load namely Load 1 was changing for 20% pu at time t=1.5 s. The load change was taken place at power grid steady station condition. The measurement data are time-series voltage/ current data from both the local and remote measurement nodes. The extracted feature vector by LSTM-AE module is fed into the RF module to estimate the magnitude and phase of the grid impedance over time.

The corresponding MSE of the estimated impedance magnitude is 1.4. Figure 6 shows the result the grid impedance magnitude estimation at fundamental frequency by the proposed method. The proposed method converged to the grid impedance after 30 ms.

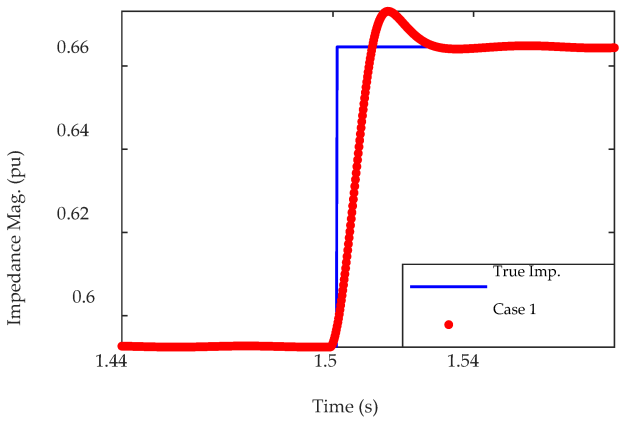

Figure 6. The result of estimating the fundamental (50 Hz) grid impedance magnitude at node B1, due to step change in Load 1, comparing with (True Imp.: true impedance).

Case Study 2: Estimation of grid impedance at harmonic frequency

The 2nd case study aimed at testing the performance of the entire scheme, where measurement data sequences from both the local and remote measurement nodes were used. After the LSTM-AE extracted the feature vector sequences and fed into the RF, the estimates of the corresponding frequency-dependent grid impedances were obtained. Table V shows the results of the proposed scheme in terms of MSE measure.

Observing the 3rd row in Table 5, MSEs of estimated impedances were of 1.3 and 3.2, respectively. For each fault location (F1 or F2) we used all corresponding 200 datapoints for test and the shown MSE in Table 5 is the average of 200 obtained individual MSEs corresponding to each datapoint. Figure 7 (a) and (b) (red traces) show the results of grid impedances estimated from the proposed scheme for two randomly datapoints corresponding to fault locations at F1 and F2, respectively.

From the results shown in Figure 7, it can be concluded that the proposed scheme can estimate the grid impedances throughout the set of selected frequency range. It is worth mentioning that only the positive sequence frequency-dependent grid impedance is shown in the figure, since the negative-sequence component presented almost identical behavior.

Table. 5. The Overall Performance of Proposed Method in Term of Mean-Square-Error (MSE) over Total Test Dataset.

	Mean Square Error	
Fault location	F1	F2
Case study 1	1.3	**3.2**
Case study 2	8.4	8.67
Case study 3	20.2	46.8

Time required for the proposed scheme: further, the time required for the proposed scheme is listed in Table 6, split according to different modules.
Observing Table 6, one can see that the training of LSTM-AE and RF took most time (180+30 min), although training was usually done once offline. While for testing process, it was fast, only requiring a total of 30 ms (1.5 grid cycle) for the combined time of feature extraction and grid impedance estimation.

Table. 6. Time Required for Training Different Modules of the Proposed Method, Feature Extraction and Impedance Estimation.

Process	Task	Time (second)
Training	LSTM-AE	10800 (or, 180 min)
Training	RF regressor	1800 (or, 30 min)
Testing	Feature extraction for one datapoint	0.02
Testing	Grid impedance estimation for one datapoint	0.01

Case Study 3: performance by using extracted features

The third case study aimed at verifying the effectiveness of using extracted features instead of using raw measurement data for RF regression. In the tests, RF regressor estimated the frequency-dependent grid impedances whereas it takes the raw data (symmetrical components) instead of extracted features as input. The resulting MSE values are shown in Table 5. Observing Table 5, one can see that without applying feature extraction (i.e., LSTM-AE module) in the proposed scheme, the MSE of the estimated impedances were 8.4 and 8.67 at points F1 and F2, respectively. The MSE values were increased for 7.1 and 5.57 as compared with the 1st case study where LSTM-AE module was used. This have demonstrated that feature extraction by LSTM-AE is effective.
To further compare the performance, Figure 7 (a) and (b), (blue traces), shows the estimated grid impedances at the same data points as that in Case study 1. Observing Figure 6, the proposed scheme without employing LSTM-AE module does not yield a relatively accurate estimation of the grid impedance. The estimation result is very close to the average of all trained datapoints. It can be considered as a RF drawback for estimating the regression function between time-series. As shown in 1st case study extracting sequences of time-dependent features of time-series helps the RF regression method to figure out the time-dependent relations between its input/ output data.

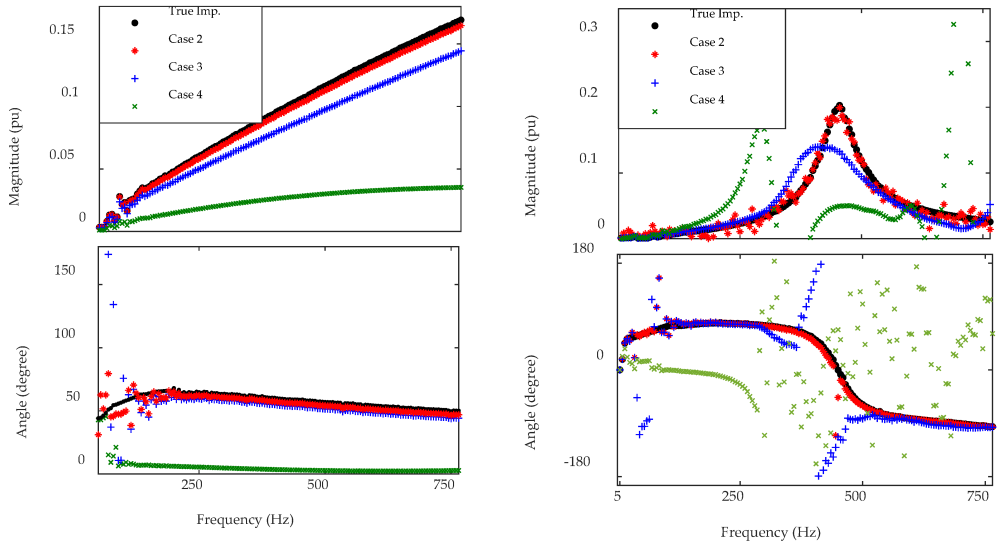

Figure 7. The result of estimating the frequency-dependent grid impedance at node B1 comparing with true impedance (True Imp) obtained by sin-sweep; (Left) three-phase fault is located at F1, impedance magnitudes (top) phase-angles (bottom), (Right) three-phase fault located at F2, impedance magnitudes (top) phase-angles (bottom).

Case Study 4: performance by using only local data

The 4th case study aimed at examining the performance impact of the proposed scheme by ignoring an additional measurement data sequence from remote locations. In this study, only the local measurements at node B1 in Figure 2 are used as an input to the LSTM-AE architecture. The 5th row of Table 5 shows the resulted MSE values of the estimated impedances. Observing the results, the MSE was 20.2 and 46.8 when the electrical faults occur in points F1 and F2, respectively. The results showed that ignoring a remotely measured data has led to dramatic change in the results.

To further compare the performance, Figure 7 (green traces) shows the estimated frequency-dependent grid impedances seen from node B1 at two random data points, same as all previous case studies. Observing the results in Figure 6, one can see that the proposed scheme cannot predict the frequency-dependent grid impedance precisely if the remote measurement data was not used. During fault occurrence the grid structure is changing adding the measurement at remote location enables proposed method to learn the grid structure.

Case Study 5: comparison with wide-band signal injection method

In the 5th case study, the performance of the proposed scheme was compared with the wide-band PRBS signal injection method [4] in terms of accuracy, frequency resolution, and speed.

In the existing method, PRBS used as the excitation signal was generated by using $f(x) = x^{15} + x + 1$, where a sequence was generated under 10 kHz sampling frequency [24]. The PRBS magnitude was set to 1% pu to avoid interfering with the transformer's no-load voltage tap-changer setting that was approximately 0.5-

1.7% on the LV side [25]. The generated PRBS signal was then added to the d-axis reference voltage (V_d) of the power converter controller. After that, the three-phase voltage and the currents were measured at the node B1 for a duration of 1.0 second. The DFT of the positive sequence components of both voltage and current were derived to estimate the positive-sequence frequency-dependent grid impedance. The time-domain signal was multiplied by the flat-top window [26] to obtain an approximate periodic signal. It is worth noting that it was not feasible to use the signal injection method for grid impedance estimation during a fault occurrence. Therefore, we compared the PRBS injection and the proposed scheme on the steady-state condition. Figure 8 (a) shows the resulting grid frequency estimates using the PRBS signal. Observing the results, the PRBS signal injection method seems to have generated good performance at frequencies below the filter's cut-off frequency which is 335 Hz. This case study was then repeated again by increasing the PRBS magnitudes to 0.1 pu, and measured the voltage signals between the RL and RC networks of the filter, like the work in [4]. Figure 8 (b) shows the obtained result, where the corresponding MSE was 1.4.

The signal injection method was not feasible during large transients. Besides, using a large magnitude for excitation signal might be harmful to other sensitive devices, and the excitation signal with a small magnitude could not be used for estimating the impedance at higher frequencies. Further, the signal injection was slower than the proposed scheme. To estimate grid impedance at lower frequencies like 5 Hz, one needs at least one-second measurement to perform an acceptable DFT spectrum where the proposed method needs only 1 gride cycle measurement data and the computation demand is 30 ms.

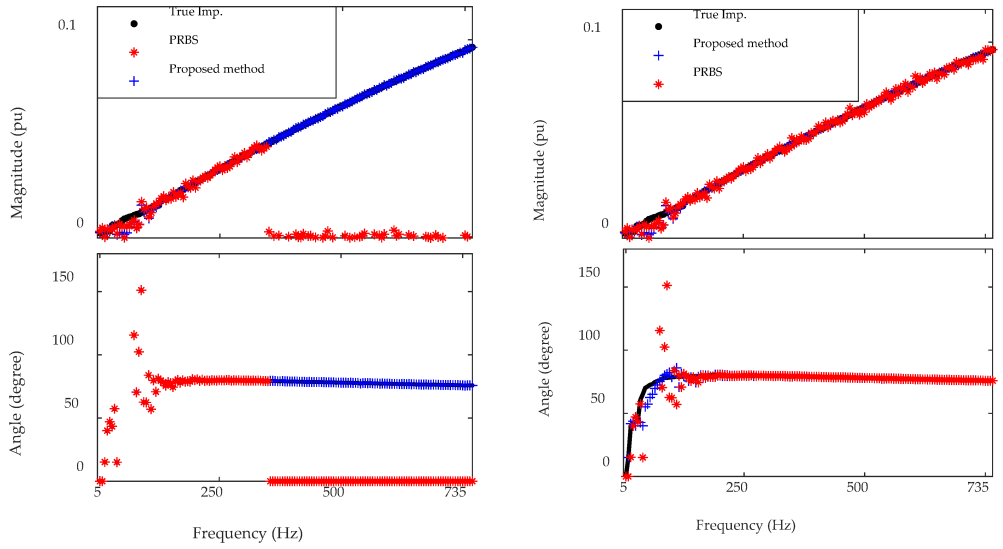

Figure 8. Case Study 5: The result of estimating the frequency-dependent grid impedance magnitude (top) and angle (bottom), at node B1, at steady state condition, by the proposed method and PRBS injection method: (Right) voltage signals were measured at node B1 and the PRBS magnitude is 0.01 pu, (Left) voltage signals were measured at point between filter's RL and RC networks, and the PRBS magnitude is 0.1 pu.

Discussion

The results show that the LSTM-AE is generally an effective method for extracting sequential features which consequently improves the RF regression technique performance. Simulation results have shown that accurate estimation of the grid impedance at the point of interest can be achieved in case of normal variations of the grid operation (for example, due to a load change). On the other hand, the results in Case study 3 and 4 show remote measurements are needed for accurate estimation of the harmonic impedance, especially in the high frequency range and close to the resonance. It is of importance to stress that adding measurements at remote nodes enables for proper estimation of the harmonic impedance also during large disturbances in the power grid, despite the fact that the RF model has been trained based on steady-state data. However, the main challenges in front of remote measurement are:

1. the latency due to data communication from remote nodes to the local node;
2. considering the related cost it is not possible to do the measurement at all nodes of the power grid;
3. there is no knowledge about the number and the location of best nodes for remote measuring.

It is worth mentioning that this project ignored the time delay in measurement data assuming that the measurement has been done under 5G internet protocols which introduce ultra-reliable-low-latency communication (URLLC) system which guarantees the reliability of 99.999% and latency less than 1 ms [27]. Future works will be using the proposed method for analysing real measured power grid data from different utility grids including several grid-connected power converters. qualitative and quantitative search for finding the best location and best number of remote measurements nodes.

Publications

1. A. Bagheri, M. Bongiorno, I. Y. Gu and J. R. Svensson, “Estimation of Frequency-Dependent Impedances in Power Grids by Deep LSTM Autoencoder and Random Forest,” Energies, 2021.
2. S. Sakar, A. Bagheri, S. Ronnberg and M. H. J. Bollen, “Susceptibility of LED street lamps to voltage dips,” Lighting Research and Technology, 2020.
3. M. Ghasemi, A. Bagheri, M. Bongiorno and J. R. Svensson, “A novel application of flywheel system to enhance fault-ride-through of the microgrids,” in proceedings of NEIS 2019 - Conference on Sustainable Energy Supply and Energy Storage Systems, 2019

References

1. Harnefors, L., Bongiorno, M., & Lundberg, S. (2007). Input-admittance calculation and shaping for controlled voltage-source converters. IEEE transactions on industrial electronics, 54(6), 3323-3334.
2. Xu, J., Xie, S., Qian, Q., & Zhang, B. (2017). Adaptive feedforward algorithm without grid impedance estimation for inverters to suppress grid current instabilities and harmonics due to grid impedance and grid voltage distortion. IEEE Transactions on Industrial Electronics, 64(9), 7574-7586.
3. Cobreces, S., Bueno, E. J., Pizarro, D., Rodriguez, F. J., & Huerta, F. (2009). Grid impedance monitoring system for distributed power generation electronic interfaces. IEEE Transactions on Instrumentation and Measurement, 58(9), 3112-3121.
4. G. Stamatiou, "Converter interactions in VSC-based HVDC systems." PhD dissertation, Chalmers University of Technology, 2017
5. Roinila, T., Vilkko, M., & Sun, J. (2013, September). Broadband methods for online grid impedance measurement. In 2013 IEEE Energy Conversion Congress and Exposition (pp. 3003-3010). IEEE.
6. Sanchez, S., & Molinas, M. (2014). Large signal stability analysis at the common coupling point of a DC microgrid: A grid impedance estimation approach based on a recursive method. IEEE Transactions on energy conversion, 30(1), 122-131.
7. Hoffmann, N., & Fuchs, F. W. (2013). Minimal invasive equivalent grid impedance estimation in inductive–resistive power networks using extended Kalman filter. IEEE Transactions on Power Electronics, 29(2), 631-641.
8. Alves, D. K., Ribeiro, R. L., Costa, F. B., & Rocha, T. O. A. (2018). Real-time wavelet-based grid impedance estimation method. IEEE Transactions on Industrial Electronics, 66(10), 8263-8265.
9. Asiminoaei, L., Teodorescu, R., Blaabjerg, F., & Borup, U. (2005). Implementation and test of an online embedded grid impedance estimation technique for PV inverters. IEEE Transactions on Industrial Electronics, 52(4), 1136-1144.
10. Ghanem, A., Rashed, M., Sumner, M., Elsayes, M. A., & Mansy, I. I. (2017). Grid impedance estimation for islanding detection and adaptive control of converters. IET Power Electronics, 10(11), 1279-1288.
11. Asiminoaei, L., Teodorescu, R., Blaabjerg, F., & Borup, U. (2005). A digital controlled PV-inverter with grid impedance estimation for ENS detection. IEEE Transactions on Power Electronics, 20(6), 1480-1490.
12. Liserre, M., Blaabjerg, F., & Teodorescu, R. (2007). Grid impedance estimation via excitation of $ LCL $-filter resonance. IEEE Transactions on Industry Applications, 43(5), 1401-1407.
13. Givaki, K., & Seyedzadeh, S. (2019). Machine learning based impedance estimation in power system.

14. Céspedes, M., & Sun, J. (2012, September). Online grid impedance identification for adaptive control of grid-connected inverters. In 2012 IEEE Energy Conversion Congress and Exposition (ECCE) (pp. 914-921). IEEE.
15. Mohammed, N., Ciobotaru, M., & Town, G. (2019). Online parametric estimation of grid impedance under unbalanced grid conditions. Energies, 12(24), 4752.
16. Gensler, A., Henze, J., Sick, B., & Raabe, N. (2016, October). Deep Learning for solar power forecasting—An approach using AutoEncoder and LSTM Neural Networks. In 2016 IEEE international conference on systems, man, and cybernetics (SMC) (pp. 002858-002865). IEEE.
17. Policardi, F. (2011). MLS and Sine-Sweep measurements. Università di Bologna, Italia ELEKTROTEHNIŠKI VESTNIK, 78(3), 91-95.
18. Srivastava, N., Mansimov, E., & Salakhudinov, R. (2015, June). Unsupervised learning of video representations using lstms. In International conference on machine learning (pp. 843-852). PMLR.
19. Sagheer, A., & Kotb, M. (2019). Unsupervised pre-training of a deep LSTM-based stacked autoencoder for multivariate time series forecasting problems. Scientific reports, 9(1), 1-16.
20. Ge, C., de Oliveira, R. A., Gu, I. Y. H., & Bollen, M. H. (2020). Deep Feature Clustering for Seeking Patterns in Daily Harmonic Variations. IEEE Transactions on Instrumentation and Measurement, 70, 1-10.
21. Statnikov, A., Wang, L., & Aliferis, C. F. (2008). A comprehensive comparison of random forests and support vector machines for microarray-based cancer classification. BMC bioinformatics, 9(1), 1-10.
22. Breiman, L. (2001). Random forests. Machine learning, 45(1), 5-32.
23. Liaw, A., & Wiener, M. (2002). Classification and regression by randomForest. R news, 2(3), 18-22.
24. Nowozin, S. (2012). Improved information gain estimates for decision tree induction. arXiv preprint arXiv:1206.4620.
25. Bagheri, A., Gu, I. Y., Bollen, M. H., & Balouji, E. (2018). A robust transform-domain deep convolutional network for voltage dip classification. IEEE Transactions on Power Delivery, 33(6), 2794-2802.
26. Barker, H. A. (2004). Primitive maximum-length sequences and pseudo-random signals. Transactions of the Institute of Measurement and Control, 26(4), 339-348.
27. Gajić, Z., & Aganović, S. (2006). Advanced tapchanger control to counteract power system voltage instability.
28. Sachs, J., Wikstrom, G., Dudda, T., Baldemair, R., & Kittichokechai, K. (2018). 5G radio network design for ultra-reliable low-latency communication. IEEE network, 32(2), 24-31.